Investigating the Effect of Seasonal Plant Growth and Development in Three-Dimensional Atmospheric Simulations. Part I: Simulation of Surface Fluxes over the Growing Season

ELENA A. TSVETSINSKAYA AND LINDA O. MEARNS

National Center for Atmospheric Research, Boulder, Colorado

WILLIAM E. EASTERLING

The Pennsylvania State University, University Park, Pennsylvania

(Manuscript received 13 December 1999, in final form 27 April 2000)

ABSTRACT

The authors examine the effect of seasonal crop development and growth on the warm-season mesoscale heat, moisture, and momentum fluxes over the central Great Plains region of North America. The effect of crop growth and development on the atmospheric boundary layer is addressed in a follow-up paper (Part II). Energy, moisture, and momentum fluxes are studied over a maize agroecosystem at the scale of a 90-km atmospheric grid cell. Daily plant development and growth functions incorporated into the surface flux calculations are based on a physiological crop growth model CERES-Maize version 3.0. CERES-Maize simulates daily plant growth and development as a function of both environmental conditions (temperature, precipitation, solar radiation, and soil moisture) and plant-specific genetic parameters. Plant growth and development functions from CERES were incorporated into the Biosphere–Atmosphere Transfer Scheme (BATS), and selected crop parameters [i.e., Leaf Area Index (LAI) and crop height] were validated against field data. The sensitivity of sensible (H) and latent (LE) heat fluxes, and momentum flux (τ) to interactively simulated LAI and canopy height was quantified.

During the extremely dry season of 1988, 20%–35% changes in sensible heat and 30%–45% changes in latent heat occurred in response to LAI changes from 5 to 1 (the values simulated in the control and interactive experiments, respectively). These changes are statistically significant (at the 0.05 level) for all the locations and years under consideration. Relative contributions of evaporation and transpiration to the latent heat flux were also strongly affected by these LAI changes. This effect had a distinct diurnal pattern, with the strongest signal seen in midafternoon hours, and was more pronounced during the dry years (e.g., 1988 and 1989) compared to the favorably moist years (e.g., 1991, 1993).

1. Introduction

There is evidence that for large vegetated areas with little relief (e.g., the Great Plains of North America) climate simulations are improved through the interactive coupling of general circulation and mesoscale climate models with plant growth and development models (Xue et al. 1996; Tsvetsinskaya et al. 1999). The significance of this research is in providing quantitative estimates of the effect of interactive representation of seasonal crop development and growth in a mesoscale climate model on the simulated heat and moisture fluxes and the structure of the planetary boundary layer (PBL) over the central Great Plains of North America.

In this paper, we first review the processes of land–atmosphere exchange and some of the modeling efforts, which have achieved our present understanding of the coupled land–atmosphere subsystems. Next, we discuss the interactive coupling of a crop model (CERES-Maize) to the Biosphere–Atmosphere Transfer Scheme (BATS; Dickinson et al. 1993) and introduce a quasi-mechanistic (combination of deterministic functions and data parameterizations) interactive version of BATS. The interactive version of BATS accounts for plant seasonal development, growth (including biomass accumulation and allocation), and senescence, responding to hybrid-specific genetic parameters and environmental conditions (i.e., temperature, radiation, and water stress). Performance of both control and interactive versions of BATS for maize is validated over selected growing seasons against field data. We discuss the effect of interactively simulated plant growth and development on seasonal and interannual variability in surface heat, moisture, and momentum fluxes. The follow-up paper (Part II) discusses the dynamic response of a high-res-

Corresponding author address: Elena Tsvetsinskaya, NCAR/ESIG, P.O. Box 3000, Boulder, CO 80307-3000.
E-mail: elena@ucar.edu

olution atmospheric model to surface forcing and examines certain conditions when plant seasonal growth can induce mesoscale circulations in the atmosphere.

The null hypothesis that we are testing is that there are no substantial differences in surface fluxes of sensible heat, latent heat, and momentum, at the scale of a 90-km atmospheric grid cell, between the current version of BATS, BATS 1e, and the interactive version of BATS, BATS-GF, which incorporates CERES crop growth and development functions.

We chose maize as an agroecosystem of interest because it is a major staple crop grown in the central United States, and it exhibits significant seasonal changes in LAI and plant height. The area of corn production in the central Great Plains varies from 55% of land in Iowa to 46% in Nebraska, 30% in South Dakota, and 15% in Kansas (United States Department of Agriculture National Agricultural Statistics Service Agricultural Handbook Number 628).

2. Research to date

Terrestrial ecosystem processes strongly respond to atmospheric temperature, humidity, precipitation, and radiative transfer, as well as to surface hydrological processes including runoff, percolation, and snowpack accumulation and melt. Atmospheric processes including mesoscale circulations and the formation of clouds and precipitating systems can be highly dependent on surface heat and moisture fluxes, which, in turn, are largely determined by live and dead vegetation and soil moisture storage. Vegetation plays a major role in determining precipitation interception, runoff, and soil moisture removal via transpiration and evaporation.

At present, the land surface is represented in most three-dimensional climate models through biophysical models that provide estimates of energy, mass, and momentum fluxes in both space and time. These models represent one-way vegetation–atmosphere interactions. Typically, a biophysical model receives a set of climate variables from either the climate model (online simulations) or from observations (offline simulations). It then calculates the surface fluxes of heat, moisture, and momentum as determined by both climate inputs and surface parameters. The number of surface parameters depends upon the complexity of the model, but typically included are albedo (α), leaf area index (LAI), canopy fractional cover (σ_f), roughness length (z_0), canopy conductance (G_s), transmittance/reflectance, and leaf orientation. Examples of biophysical models include BATS (Dickinson et al. 1993), Simple Biosphere Model (SiB; Sellers et al. 1986), Land Surface Model (LSM; Bonan 1996), Land-Surface-Transfer Model (LSX; Pollard and Thompson 1995), and Canadian Land Surface Scheme (CLASS; Verseghy et al. 1993).

To account for spatial differences in surface parameters, biophysical models distinguish between a certain number of land cover types (18 in the case of BATS) and prescribe vegetation attributes to each type. These vegetation parameters are usually assigned as mean values for a given land cover type, or vary in accordance with simple climatologically prescribed functions (e.g., in BATS LAI is determined solely by subsoil temperature with no regard for soil moisture status). Examples of land cover classes include crop, irrigated crop, grassland, evergreen forest, desert, etc. The compilation of the 0.5° dataset of land cover types used in this study is described in Dickinson et al. (1993); the dataset is based on Olson et al. (1983).

Recently, the most advanced surface models have attempted to represent seasonal variability through incorporating remotely sensed data to provide estimates of LAI and possibly soil moisture content as inputs into the surface models (Collatz et al. 1993; Sellers et al. 1992). Prescription of LAI from Advanced Very High Resolution Radiometer (AVHRR) data improves estimates of mass and energy fluxes for the present climates for which such data are available since it allows for the mimicking of the seasonal cycle of vegetation growth and hence increases the realism of bioatmospheric flux parameterizations (Ciais et al. 1995). While adding a great deal of realism to climate simulations, such an approach is limited to the short window of time for which remotely sensed data are available and cannot be used for long-term climate studies or sensitivity experiments such as $2 \times CO_2$ climate simulations.

In most land surface models to date, plant growth (both above- and below-ground biomass accumulation and allocation) and development are poorly if at all represented. Such coarseness of vegetation models often results in biases in surface parameter calculations that are passed on to the atmospheric model. The failure to adequately represent root growth, for example, translates into the inability to simulate the conservation of soil moisture early on in the growing season that is used later in the summer, which skews regional-scale latent heat flux and precipitation calculations (Beljaars et al. 1996; Viterbo and Beljaars 1995).

Another problem is that land surface models poorly represent agroecosystems. All agricultural crops, including such different crops as corn, wheat, and rice for example, are treated as one and the same land cover category, crops. The only distinction made is between irrigated and nonirrigated agriculture. Yet a number of studies made use of these models to evaluate the effect of land cover changes from forests and grasslands to agriculture on the climate of the North America and other regions (Chase et al. 1999; Bonan 1997; Copeland et al. 1996).

Interactive coupling between atmospheric and terrestrial vegetation models is a relatively new endeavor. First attempts to incorporate interactive vegetation into surface models have been undertaken by Foley et al. (1996), Dickinson et al. (1998), and Lu et al. (2001). None of these groups, however, explicitly addressed the issue of detailed representation of agroecosystems. The

value of our study is in that we focus explicitly on agroecosystem simulations, and thus represent the actual landscapes of the central Great Plains with a higher degree of realism.

In spring when many agricultural crops are planted and begin foliage production, the appearance of leaves triggers a rapid increase in transpiration (Schwartz and Karl 1990) and changes in surface albedo. As plants grow and LAI changes, consequent changes in surface albedo, bulk canopy conductance, and roughness length occur, accompanied by changes in surface fluxes of sensible and latent heat and momentum. Experimental data indicate that at least some biophysical parameters (LAI canopy height, bulk canopy conductance, fractional canopy cover) vary significantly throughout the growing season (five-fold changes). Such changes have a noticeable effect on the fluxes of sensible and latent heat, which is confirmed by many observational (Kim and Verma 1990; Verma et al. 1992) and modeling (Bonan et al. 1993; Viterbo and Beljaars 1995) studies. Subsequently, the thermodynamic properties of the atmospheric boundary layer are altered (Betts et al. 1993; Schwartz 1992) including daily maximum air temperature, lower-atmospheric lapse rate, surface vapor pressure, and relative humidity. In drought years in the Midwest and the Great Plains of North America, such as 1988 and 1989, extensive plant wilt in response to severe moisture stress has been suggested to act as a positive feedback mechanism to drought intensification (Trenberth and Branstator 1992; Trenberth and Guillemot 1996) by reducing evapotranspiration, and as a negative feedback mechanism to drought duration by more rapidly eliminating the original soil moisture deficit. Thus, by neglecting the effect of drought-stressed vegetation in land surface models, the severity of droughts is likely to be underestimated and their duration overestimated (Dirmeyer 1994).

The principal objective of this paper is to investigate the effect, over a predominantly agricultural central U.S. domain, of crop development and growth on the warm-season mesoscale sensible and latent heat fluxes. The follow-up paper (Part II) explores the effect of the resultant changes in surface fluxes on the atmospheric boundary layer (ABL). In order to address the above-stated objective, the National Center for Atmospheric Research Regional Climate Model (NCAR RegCM)/BATS configuration was interactively coupled to a physiologically based crop model (CERES-Maize). We strived to develop a comprehensive agroecosystem–hydrological–atmospheric model, which would allow interactive studies of the mesoscale climate, local, and mesoscale soil moisture changes and ecosystems over predominantly agricultural domains (i.e., the Great Plains and Midwest regions of the United States). Some results of Mearns et al. (1996, 1997) suggest the potential importance of representing two-way agroecosystem–climate interactions over predominantly agricultural central United States.

TABLE 1. Crop parameters from Dickinson et al. (1993). R_{smin} is the minimum stomatal resistance (s m^{-1}); LAI is the leaf area index (nondimensional); SAI is the stem area index (nondimensional); z_0 is the roughness length (m); α is the vegetation albedo (in the visible and near-infrared portions of spectrum); $\sigma_{f\max}$ is the maximum fractional vegetation cover (nondimensional).

BATS class	R_{smin}	LAI max/min	SAI	z_0	α vis/NIR	$\sigma_{f\max}$
Crop	120	6.0/0.5	0.5	0.06	0.1/0.3	0.85
Irrigated crop	200	6.0/0.5	2.0	0.06	0.08/0.28	0.80

Through a robust representation of seasonal changes in plant development and growth and associated changes in local and mesoscale soil moisture patterns, we will demonstrate the effect of the interactively simulated LAI and canopy height on model-simulated sensible and latent heat fluxes and momentum flux and on mesoscale atmospheric circulations and ABL structure over the central United States. Both interactive and control simulations were conducted in two modes: stand-alone runs driven with observed weather (described in this paper) and runs coupled to the National Center for Atmospheric Research Regional Climate Model (described in a follow-up paper, Part II). We validated results of this modeling study against field data over the central United States. In a broad sense, this research should improve our understanding of the factors controlling seasonal variability in land surface hydrology and mesoscale climate over the central Great Plains region of North America.

3. Model description

Two models were employed in this study, the Biosphere–Atmosphere Transfer Scheme version 1e, BATS-1e, and CERES-Maize version 3.0. The physical parameterizations employed by BATS are described in detail in Dickinson et al. (1993). The detailed description of the CERES-Maize model can be found in Jones and Kiniry (1986). Here we provide a brief summary for each model.

a. BATS 1e model description

BATS is a surface physics/soil hydrology model that incorporates a vegetation layer, three soil layers for moisture, and two soil layers for temperature. At an atmospheric model grid point, a vegetation class is assigned, which is defined by several parameters including maximum and minimum LAI, stem area index (SAI), minimum stomatal resistance (R_{smin}), and maximum fractional vegetation cover ($\sigma_{f\max}$). These parameter values for agroecosystems, the vegetation class simulated in this study, are given in Table 1.

A schematic representation of the components of the surface sensible and latent heat flux calculations is given in Fig. 1. BATS assumes that a grid cell is composed

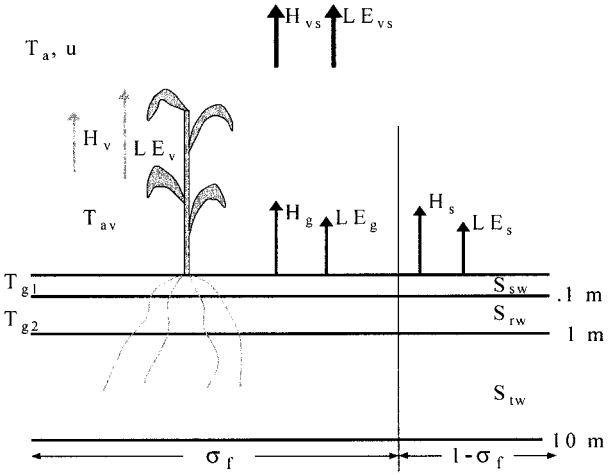

FIG. 1. Sensible and latent heat fluxes in BATS.

of a homogeneous mixture of a single vegetation class and bare soil. The net fluxes from a grid cell (H, LE) are computed as the means from bare soil (H_s, LE_s) and vegetation (H_{vs}, $\mathrm{LE}_{\mathrm{vs}}$), weighted by the fractional area ($1 - \sigma_f$ and σ_f, respectively) covered by each. The fluxes from the vegetated fraction of a grid cell are the sum of fluxes from the ground below the canopy (H_g, LE_g) and those from the canopy (H_v, LE_v).

Sensible heat fluxes from the vegetated fraction of a grid cell are computed as

$$H_{\mathrm{vs}} = H_v + H_g, \tag{1}$$

where

$$H_{\mathrm{vs}} = \rho_a \sigma_f C_p C_D u (T_{\mathrm{av}} - T_a), \tag{2}$$

$$H_v = \rho_a \sigma_f C_p (L + S) r_{\mathrm{la}}^{-1} (T_v - T_{\mathrm{av}}), \quad \text{and} \tag{3}$$

$$H_g = \rho_a \sigma_f C_p C_{\mathrm{SOILC}} u_v (T_{\mathrm{gl}} - T_{\mathrm{av}}). \tag{4}$$

In this formulation, u is the wind speed at the lowest atmospheric level; u_v is the wind speed within the canopy; ρ_a is the density of surface air; σ_f is the fractional vegetation cover for each grid cell; C_p is the specific heat of air; C_D is the surface drag coefficient; C_{SOILC} is the transfer coefficient between the canopy air and underlying soil (C_{SOILC} is assumed to be 0.004, see Dickinson et al. 1993); L is the leaf area index; S is the stem area index; r_{la}^{-1} is the aerodynamic resistance between leaves and air; T_a is the air temperature above canopy; T_{av} is the canopy air temperature; T_v is the canopy temperature; T_{g1} and T_{g2} are the temperatures of the surface and subsurface soil layers, respectively.

Similarly, latent heat flux from the vegetated fraction of a grid cell is calculated as

$$\mathrm{LE}_{\mathrm{vs}} = \mathrm{LE}_v + \mathrm{LE}_g, \tag{5}$$

where

$$\mathrm{LE}_{\mathrm{vs}} = \rho_a \sigma_f C_D u (q_{\mathrm{av}} - q_a), \tag{6}$$

$$\mathrm{LE}_v = \rho_a r_{\mathrm{la}}^{-1} r'' (q_v^{\mathrm{SAT}} - q_{\mathrm{av}}), \quad \text{and} \tag{7}$$

$$\mathrm{LE}_g = \rho_a C_{\mathrm{SOILC}} \sigma_f u_v f_g (q_g^{\mathrm{SAT}} - q_{\mathrm{av}}). \tag{8}$$

In this formulation, q_a is the specific humidity of the lowest atmospheric layer; q_{av} is the specific humidity of canopy air; q_v^{SAT} is the saturated specific humidity at canopy temperature; q_g^{SAT} is the saturated specific humidity at soil surface temperature; f_g is the ground wetness factor, defined as the ratio of actual to potential ground evaporation; and r'' is the fraction of potential evaporation from the leaf. Calculation of r'' includes transpiration from the dry fraction of the canopy, the effect of canopy resistance, and accumulated dew on the leaves:

$$r'' = 1 - \delta(E_f^{\mathrm{WET}}) \left[1 - L_W - L_d \left(\frac{r_{\mathrm{la}}}{r_{\mathrm{la}} + r_s} \right) \right], \tag{9}$$

where r_s is stomatal resistance and is a function of temperature, radiation, soil moisture, and vapor pressure deficit; δ is a step function and is 1 for positive argument and 0 for nonpositive argument; L_W is the ratio of wetted leaf–stem area to total leaf–stem area exchanging water with the atmosphere; L_d is the unwetted fraction of leaf–stem area free to transpire. Here, E_f^{WET} is the evaporation of water on wet foliage (leaves and stems) per unit wetted area and is calculated as (each term of this equation is defined above)

$$E_f^{\mathrm{WET}} = \rho_a r_{\mathrm{la}}^{-1} (q_v^{\mathrm{SAT}} - q_{\mathrm{av}}). \tag{10}$$

The surface area of vegetation per unit area of ground consists of leaf area index (L), or transpiring leaf surfaces, and stem area index (S), or nontranspiring surfaces. In BATS, the stem area index is a constant for each land type, whereas leaf area index has a seasonal variation. Seasonal LAI is calculated as a quasi-climatologically prescribed function of subsoil temperature, T_{g2} [see Dickinson et al. (1993) for details]:

$$L = L^{\mathrm{MIN}} + F_{\mathrm{SEAS}}(T_{\mathrm{g2}}) \cdot (L^{\mathrm{MAX}} - L^{\mathrm{MIN}}), \tag{11}$$

where

$$F_{\mathrm{SEAS}}(T_{\mathrm{g2}}) = 1 - 0.0016(298.0 - T_{\mathrm{g2}})^2 \tag{12}$$

when

$$273.16 < T_{\mathrm{g2}} < 298.$$

The fluxes from bare soil are computed using the standard bulk transfer method,

$$H_s = \rho_a C_p C_D u (T_{\mathrm{gl}} - T_a), \tag{13}$$

$$\mathrm{LE}_s = \rho_a C_D u f_g (q_g - q_a), \quad \text{and} \tag{14}$$

$$\tau = \rho_a C_D u^2. \tag{15}$$

The soil moisture calculations include predictive equations for water content of the surface soil layer, the root zone, and the deep soil layer corresponding to

TABLE 2. Crop genetic parameters used as inputs for CERES-Maize.

P1	P2	P5	G2	G3	PHINT
300.0	0.7	700.0	650.0	8.5	75.0

depths of 0.1, 1, and 10 m, respectively. BATS soil texture classes ranging from 1 (sand) to 12 (clay) are derived from the Zobler World Soil Data File (Zobler 1986) and the Goddard Institute for Space Studies (GISS) Global Data Set of Soil Particle Size Properties (Webb et al. 1991).

b. CERES v3.0 model description

CERES (Crop Estimation through Resource and Environment Synthesis)-Maize version 3.0 (Jones and Kiniry 1986; Tsuji et al. 1994) is a physiologically based comprehensive crop model. It calculates crop phasic development and dry matter accumulation and allocation between plant parts based on genetic and weather information. The CERES family of models uses a daily time step and simulates growth and development of such crops as maize, wheat, sorghum, and rice as well as C3 and C4 grasses. In this study we used the maize model of the CERES family. It has been validated over the central Great Plains of the United States (Kiniry et al. 1997; Pang et al. 1997) and has been applied to numerous climate change impact analyses (Mearns et al. 1999; Rosenzweig 1990).

CERES requires four kinds of input data: (a) daily weather data, (b) plant genetic coefficients, (c) soil data, and (d) management. Weather inputs are daily solar radiation (MJ m^{-2} day^{-1}), maximum and minimum air temperature (°C), and precipitation (mm day^{-1}). Genetic inputs are coefficients related to photoperiod and temperature sensitivity. They are cultivar-specific and include (i) thermal time from seedling emergence to the end of the juvenile phase (P1), expressed in degree days above the base temperature of 8°C; (ii) extent to which development is delayed for each hour increase in photoperiod above the longest photoperiod at which development proceeds at a maximum rate (P2), expressed in days; (iii) thermal time from silking to physiological maturity (P5), expressed in degree days above the base temperature of 8°C; (iv) maximum possible number of kernels per plant (G2); (v) kernel filling rate during the linear grain filling stage and under optimum conditions (G3, mg day^{-1}); and (vi) phylochron interval (PHINT), the interval in degree days between successive leaf tip appearances. Genetic coefficients used in this study are given in Table 2. They are based on Pioneer3382 hybrid and adjusted to achieve a better agreement with field data.

Soil inputs include soil albedo, soil depth, drainage and runoff coefficients, evaporation limit, soil water holding capacity amounts, and rooting preference coefficients at several depth increments. CERES also requires that saturated soil water content and initial soil water content (soil water content on the first day of simulation) be specified. Management inputs are plant population density, planting depth, and date of planting. If irrigation is used, the date of application and amount should be specified. Latitude of the site should be specified as well.

TABLE 3. Maize growth stages as simulated in CERES v3.0.

Stage number	Event	Plant parts growing
7	Fallow or presowing	
8	Sowing to germination	
9	Germination to emergence	Roots, coleoptile
1	Emergence to the end of juvenile	Roots, leaves
2	End of juvenile to floral initiation	Roots, leaves, stems
3	Floral initiation to 75% silking	Roots, stems, ear
4	75% silking to beginning of grain fill	Roots, stems
5	Beginning of grain fill to maturity	Roots, stems, grain
6	Maturity to harvest	

CERES-Maize incorporates the fundamentals of light interception by crops, the uptake of carbon dioxide and its conversion to biomass, and the partitioning of the biomass into the growing organs of the plants, as well as the losses of biomass to respiration and death of plant organs. At the core of CERES-Maize there is a crop growth submodel, which incorporates such physiological processes as: 1) carbon assimilation (photosynthesis); 2) carbon loss (respiration); and 3) carbon allocation (partitioning). Plant growth is usually simulated for optimum conditions, and then various stresses (nutrient, water, heat, etc.) are imposed.

In this paper we focus on the aspects of CERES-Maize that deal with the simulation of plant phasic development, and plant growth and organ development. Phasic development in CERES v3.0 deals with the duration of growth stages. The growth stages are organized around times in the plant life cycle when changes occur in partitioning of assimilate among different plant organs. The growth stages are numbered between 1 and 9. Stages 1–5 are active above-ground growing stages and the remainder are used to describe other important events in the crop cycle. The growth stages for maize are represented in Table 3.

Phasic development in CERES v3.0 is influenced by both genotype and environment. Genotypic coefficients used in this study are given in Table 2. The key environmental variables are temperature, soil moisture (for germination), and day length (for flowering). It is assumed that development rates are directly proportional to temperature in the range from the base (8°C for maize) to some maximum (34°C for maize) temperature. Thus daily temperature above 8°C is accumulated and is referred to as thermal time. When the minimum temperature is above the base temperature and the maximum is below 34°C, thermal time for a day is assumed to be

the mean of the two values. If either the maximum or the minimum temperature is outside of this range, a separate thermal time calculation is made using the mean temperature and temperature range.

Phasic development is also a function of photoperiod. Photoperiodic induction is assumed to decrease with increasing photoperiod for photoperiods greater than 12.5 h. The number of days of tassel initiation delay for each hour increase in photoperiod is assumed to be a constant for any given photoperiod-sensitive cultivar.

After the growth stage has been determined, dry matter accumulation by individual plants is calculated and allocated between different plant parts (i.e., leaves, stems, roots, grain). First, potential dry matter production (PCARB, *g*/plant) is calculated as a function of photosynthetically active radiation (PAR), plant population (PLANTS) specified a priori, and LAI:

$$\text{PCARB} = \frac{5.0\text{PAR}}{\text{PLANTS}}[1 - \exp(-0.65\text{LAI})].$$

This equation implies that leaf interception of PAR obeys Beer's law, the extinction coefficient is 0.65, and 5.0 g of dry biomass is produced per MJ of intercepted PAR under nonstressed conditions. The actual rate of dry matter production (CARBO) is a function of the potential rate decremented by moisture (SWFAC), temperature (PRFT), or nutrient (NSTRESS) stress:

$$\text{CARBO} = \text{PCARB} \times \min(\text{SWFAC, PRFT, NSTRESS}).$$

The actual accumulated biomass is then partitioned between plant parts (leaves, roots, stems, grain). This partitioning is highly growth-stage-specific. We use growth stage 1 here as an example. After emergence and before the end of juvenile stage (stage 1) all biomass is partitioned between leaves and roots. When the leaf number is less than 4.0, daily growth of leaf area per plant (PLAG) is a function of leaf number (XN); the fraction of a leaf emerging on a day (TI), and a zero-to-unity water deficit factor for plant cell expansion (TURFAC):

$$\text{PLAG} = 3.0 \cdot \text{XN} \cdot \text{TI} \cdot \text{TURFAC}.$$

When the leaf number is greater or equal to 4.0:

$$\text{PLAG} = 3.5 \cdot \text{XN} \cdot \text{XN} \cdot \text{TI} \cdot \text{TURFAC}.$$

Total plant leaf area (PLA) is then updated:

$$\text{PLA} = \text{PLA} + \text{PLAG}.$$

PLA is set to zero at the beginning of a growing season.

New accumulated leaf weight (XLFWT) for current day is calculated next:

$$\text{XLFWT} = \left(\frac{\text{PLA}}{267.0}\right)^{1.25}.$$

The daily rate of leaf growth (GROLF) is calculated from XLFWT and the previous day's value of leaf weight (LFWT):

$$\text{GROLF} = \text{XLFWT} - \text{LFWT}.$$

Since only leaves and roots are growing during this phenological stage (between emergence and end of juvenile period), daily root growth (GRORT) is the difference between the actual dry matter production on the day (CARBO) and GROLF:

$$\text{GRORT} = \text{CARBO} - \text{GROLF}.$$

If GRORT is less than (0.25 CARBO), reserve carbohydrate in the germinated seed (SEEDRV) is used to maintain the rate of root growth, and SEEDRV is reduced accordingly.

Finally, total leaf senescence since emergence due to normal phenological development (SLAN) is calculated as a function of growing degree day accumulation (SUMDTT) and total PLA:

$$\text{SLAN} = \text{SUMDTT} \cdot \text{PLA}/10\,000.$$

Senescence is initially slow, increasing as the plant approaches physiological maturity. In addition to natural senescence with normal phasic development, low temperature, water deficit, and competition for light in dense canopies can accelerate senescence.

During later growth stages, CARBO is partitioned not only between leaves and roots but also stems, ears, and grains. After biomass accumulation and allocation are simulated on a plant level, they are scaled up to canopy level as a function of plant population density specified a priori. Leaf area index is calculated as a function of the total amount of PLA that has been produced, the total plant leaf area that has senesced (SENLA), and PLANTS:

$$\text{LAI} = 0.0001(\text{PLA} - \text{SENLA}) \cdot \text{PLANTS}.$$

As shown above, plant leaf area has an important influence on light interception and dry matter production. The rate of leaf area expansion is a component of plant growth that is quite sensitive to environmental stresses. For example, leaf growth is more sensitive to water stress than is photosynthesis. In addition, the optimum temperature for leaf growth is several degrees higher than for photosynthesis. Thus, cool temperatures or moderate drought stresses reduce expansion growth more than photosynthesis is reduced, causing increases in specific leaf weight and increasing the proportion of assimilate partitioned to roots. CERES accounts for these plant responses by using separate relationships to calculate the influence of temperature and water stress on photosynthesis and leaf growth.

CERES v3.0 calculates the soil water balance for a layered soil in order to determine reduction in growth rate caused by soil water deficits. For multiyear simulations, it also calculates the soil water when the crop is not growing, enabling the calculation of soil moisture accumulation from the practice of fallowing. Evapo-

transpiration in the model (which is divided into plant transpiration and soil evaporation components) is driven by solar radiation and temperature, based on the equilibrium evapotranspiration concept (Priestly and Taylor 1972). The water content of multiple soil layers is calculated based on changes in evaporation, root absorption, and flow to adjacent layers. Runoff is calculated using the USDA Soil Conservation Service Curve method (Williams et al. 1982).

Three soil water deficit factors are defined based on layer water contents that are then used to modify root growth, photosynthesis and transpiration, and leaf and stem growth. These are unitless numbers ranging from 1 (no stress) to 0 (maximum stress). The soil water deficit factor 1 (SWFAC) affects photosynthesis and transpiration. It is defined as the ratio of total daily root water uptake from the soil and potential plant evapotranspiration. The soil water deficit factor 2 (TURFAC) is used to determine the reduction in plant cell expansion and is calculated similar to SWFAC. The soil water deficit factor 3 (SWDF) is used to calculate root growth and water uptake. It is defined as the ratio of available soil water (actual soil water content minus soil water content at wilting point) to extractable soil water content for a given soil layer, which is defined as the difference between the soil water content at field capacity and the soil water content at wilting point.

4. Materials and methods

Ten years of weather data (1986–95) were examined for seven locations in central and eastern Nebraska and eastern Kansas: Lincoln, Mead, Clay Center, Concord, West Point, Grand Island, and Manhattan. The years were subdivided into two categories: (a) dry years, and (b) years with normal and above normal precipitation. Two criteria were used to classify the data: the total amount of precipitation during the growing season (as compared to the 10-yr mean and standard deviation), and the 6-month (1 April–30 September) Standardized Precipitation Index (SPI; McKee et al. 1993). Over the central Great Plains, the years 1988 and 1989 were drier than normal, whereas the rest of the years had normal to above-normal precipitation (note the flood year of 1993). SPI values for 1988 and 1995, a dry and a normal year, respectively, are shown in Figs. 2a,b.

We ran a 10-yr (1986–95) simulation with CERES v3.0 crop model. The input weather data, which includes incoming solar radiation (W m^{-2}), daily maximum and minimum air temperature (°C), and precipitation (mm), were obtained from the Automated Weather Data Network (AWDN; Hubbard 1994) stations operated by the High Plains Climate Center of the University of Nebraska—Lincoln. The weather data had been collected at 1-min time intervals by the AWDN stations, and averaged over a daily time step, necessary to drive CERES. The genetic coefficients used in this study are specified in Table 2 and are typical for maize hybrids grown in the central Great Plains (Kiniry et al. 1997; Jones and Kiniry 1986). The soils differed between locations gravitating toward medium silty loam in the east and medium sandy loam in the west. The soils used in BATS were tuned to CERES soils (e.g., sand to silt to clay ratio, soil albedo). Planting dates varied between locations from 20 April to 4 May. Dryland (no irrigation) option with 200 kg of nitrogen per hectare was used.

In order to estimate the effect of LAI and plant height changes on the fluxes of heat, moisture, and momentum, we performed a series of experiments with BATS. We selected three years: a dry year, 1988, a wet year, 1993, and a relatively normal year, 1995. For each of the three years, BATS was driven with the observed weather data in a manner similar to that of CERES (described above), but at an hourly time step. The weather data included incoming solar radiation (W m^{-2}), air temperature (°C) measured at anemometer (1.5 m) height, and precipitation (mm). The soil moisture in BATS was initialized at field capacity. The model was run twice for each year in a consecutive mode to allow the soil moisture to equilibrate for each of the weather scenarios. The output of the second consecutive year run was then analyzed. For each of the three years, we tested the sensitivity of BATS-simulated sensible and latent heat fluxes to changes in the LAI, and the sensitivity of BATS-simulated momentum flux to changes in surface roughness length associated with the canopy height changes. The list of LAI-sensitivity experiments is given in Table 4 and the list of surface roughness length-sensitivity experiments is given in Table 5.

5. Results and discussion

a. Incorporating ''growth function'' into BATS

We incorporated CERES formulations of maize phenological development and growth [hereafter referred to as the ''growth function'' (GF)] into BATS. This enabled BATS to account for, among other factors, the effect of moisture stress on maize development and growth.

Under no moisture stress conditions, a complete agreement between CERES-simulated LAI and BATSGF-simulated LAI is seen for all the years and all the locations (not shown here). This was expected since both models incorporate the same algorithms to simulate maize development and growth, and under conditions of no moisture stress LAI in both CERES and BATS-GF is a function of solar radiation and air temperature only. Both CERES and BATS-GF were driven with the same input weather dataset (which included solar radiation and air temperature) compiled from AWDN station data. Under limiting soil moisture conditions, the degree of water stress experienced by plants is an additional variable affecting plant development and growth. The two variables in CERES and BATS-GF that

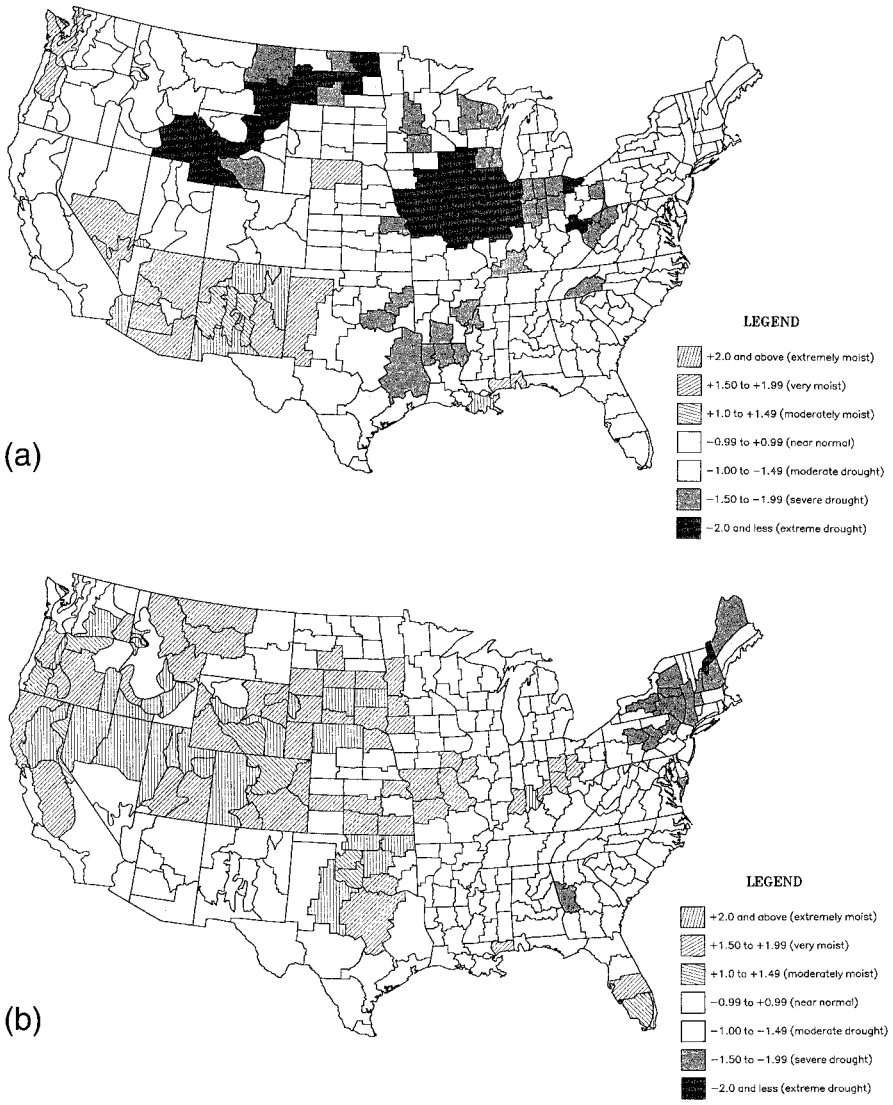

FIG. 2. Six-month (Apr–Sep) standardized precipitation index (SPI) for (a) 1988 and (b) 1991.

determine the effect of water stress on plant growth, SWFAC and TURFAC, were allowed to vary in response to changing soil moisture conditions. In CERES, SWFAC is defined as the ratio of total root water uptake to potential transpiration, and TURFAC is set to 0.67 SWFAC. In BATS, there are no parameter analogues to total root water uptake. Also, only three soil layers are allowed for soil water balance calculations and only two of them are in the root zone. Therefore, in BATS-GF we defined SWFAC and TURFAC in another way, but closest to the CERES formulations. After many tests over the domain of interest we came up with the following formulations:

TABLE 4. List of experiments conducted to test the sensitivity of BATS to LAI changes. LAI is leaf area index; SAI is stem area index; R_{smin} is minimum stomatal resistance; z_0 is roughness length; σ_{fmax} is maximum fractional canopy cover.

	Parameters of interest				
Experiment	LAI	SAI	R_{smin}	z_0	σ_{fmax}
1. Jun 1988 2. Jul 1988 3. Jul 1993 4. Jul 1995	0–6	0.1 for LAI = 0 0.5 for LAI = 1–6	120 s m^{-1}	0.06 m	0.85

TABLE 5. List of experiments conducted to test the sensitivity of BATS to roughness length (z_0) changes.

	Parameters of interest				
Experiment	LAI	SAI	R_{smin}	z_0	σ_{fmax}
1. Jun 1988 2. Jul 1988 3. Jul 1993 4. Jul 1995	4	0.5	120 s m^{-1}	0.06 m vs 0.2 m	0.85

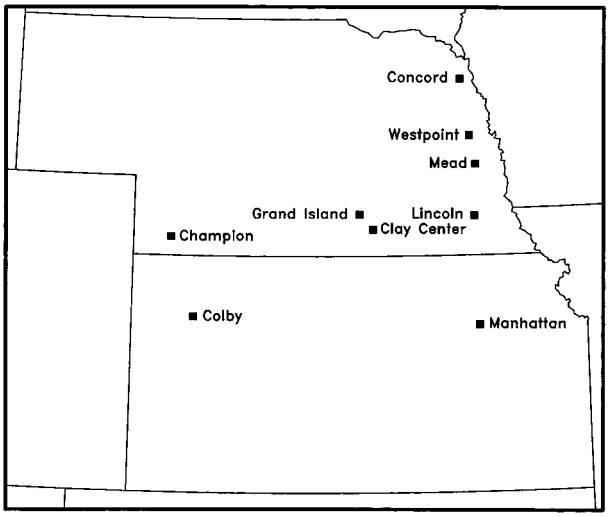

FIG. 3. Automated weather data network (AWDN) stations where BATS-GF and CERES were compared.

$$\text{SWFAC} = \frac{\text{soil water} - \text{wilting point}}{\text{field capacity} - \text{wilting point}}.$$

Thus, this modified form of SWFAC is essentially the ratio of available soil water to maximum available soil water, and

$$\text{TURFAC} = 0.67\ \text{SWFAC}.$$

Figure 3 shows the locations around the domain where the above relationships were tested. There is a generally good agreement between CERES-simulated LAI and BATSGF-simulated LAI at all the locations in 1986–95 (Fig. 4 shows the case for Grand Island for three distinctly different years). The agreement was best during the years with moderate to low water stress, 1993 and 1995. Under strong water deficit conditions (1988, 1989) the agreement was still generally good, but more discrepancies were observed. During the dry years (1988–89), maximum values of LAI varied between 1 and 3, depending on the location, whereas during the years of abundant precipitation (1987, 1990, 1992, 1993, 1995), LAI peaked at about 4. No such trend in LAI is observed in the case of BATS because the formulation of LAI in the model does not account for moisture stress (see section 3a).

Figure 5 compares LAI simulated by CERES, BATS, and BATS-GF models to actual LAI observed during the 1994–96 field experiments by J. Lindquist (Lindquist 1997) of the Department of Agronomy, University of Nebraska at Lincoln. For all three years, LAI values simulated by CERES and BATS-GF models are much closer to the observed values than is BATS-simulated LAI.

It should be noted that significant limitations of BATS related to the coarseness of its soil water balance formulation limited our ability to adequately represent root growth. There are essentially only two soil layers in the root zone in BATS and there are inherent problems with Clapp and Hornberger (1978) soil moisture potential formulation employed in BATS (Cuenca et al. 1996; Ek and Cuenca 1994). The Clapp and Hornberger (1978) functions were developed based on analysis of soil samples taken from several locations throughout the United States, but only 80% of the initial samples were used in the final analysis. The rest were discarded as they deviated significantly from the proposed function and were felt to lie beyond the bounds of reasonable expectation. The limitations of BATS have been acknowledged and are being addressed by other researchers (Dickinson et al. 1998). During the next stages of this project we plan to address this issue explicitly by substituting BATS soil water balance submodel with that of CERES.

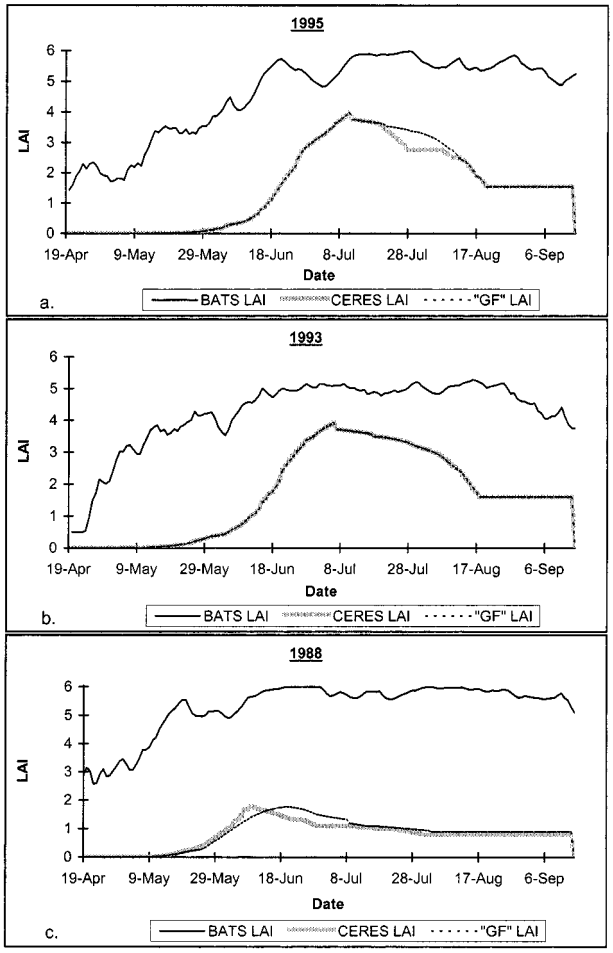

FIG. 4. Leaf area index (LAI) simulated by BATS, CERES, and BATS-GF (accounting for moisture stress) for Grand Island, NE.

b. Sensitivity of BATS-simulated sensible and latent heat fluxes to incorporating CERES development and growth functions

The net radiation received at the surface is generally balanced by outgoing fluxes of latent (LE) and sensible

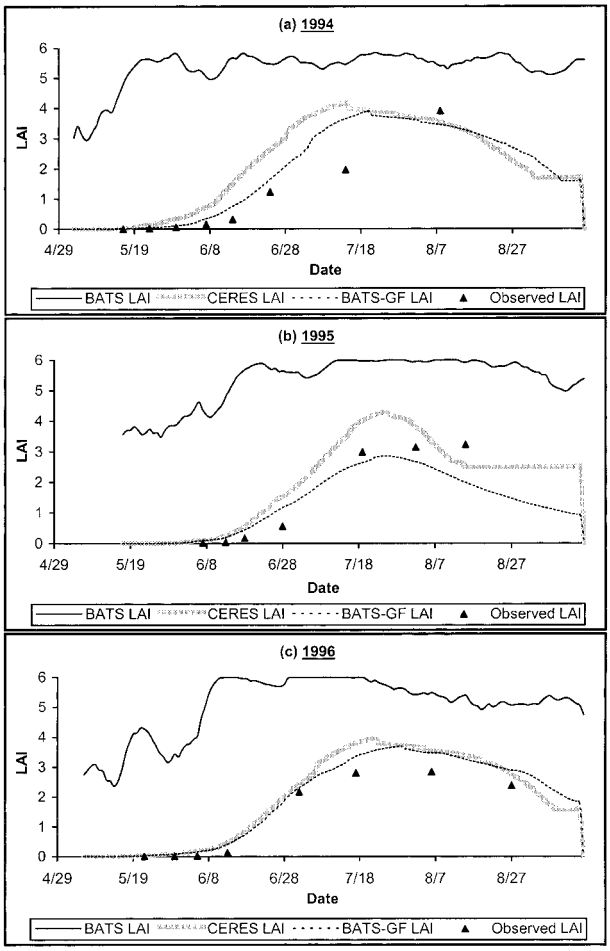

FIG. 5. Simulated and observed LAI for Mead, NE.

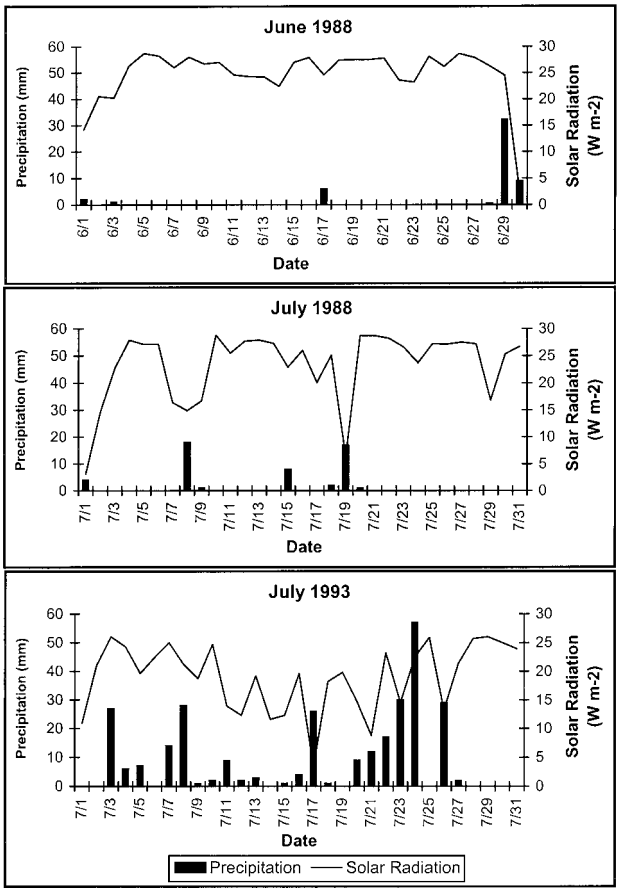

FIG. 6. Incoming solar radiation and precipitation for Grand Island, NE.

(H) heat and a downward flux into the soil (G) below the surface,

$$R_{\text{net}} = H + \text{LE} + G.$$

Over a diurnal cycle or longer, G averages to be a relatively small term, generally not more than 10% of R_{net}. For this to be the case, the sum of the outgoing sensible and latent heat fluxes must nearly equal the energy received at the surface. The magnitude of the ratio of sensible to latent heat flux, the Bowen ratio ($B = H/\text{LE}$), can be important in characterizing local and regional climate. Sensible heating of surface air creates greater instability and can result in more turbulent mixing and vertical growth of the daytime boundary layer. The energy stored in water vapor is transported vertically from the surface as latent heat flux, which is a significant source of energy in driving convection and storms. Since these two modes of heat release have very different effects on the internal heating and radiative properties of the atmosphere, the accuracy with which incoming solar energy is partitioned into these outgoing fluxes can be quite important for the realism of atmospheric simulations. The partitioning of R_{net} into H, LE, and G has been one of the most difficult problems in constructing land surface schemes (Sellers 1992).

To investigate the sensitivity of BATS-simulated sensible and latent heat fluxes to changes in Leaf Area Index, we conducted four sets of experiments (see Table 4). In each of these experiments, BATS was driven with the actual weather data observed by an AWDN station located in Grand Island, Nebraska. The same three years were considered: 1988 (a dry year), 1993 (a year of higher than normal precipitation), and 1995 (a year with precipitation around the mean). The driving weather conditions for June and July 1988 and July 1993 are given in Fig. 6 to show the sharp contrasts between the years. We also note here that such strong interannual variability in precipitation is a known factor over the central Great Plains. In July 1988, the weather station recorded only 51 mm of precipitation whereas in July 1993, the monthly total precipitation was 287 mm. Low cloudiness in July 1988 (only 7 days with precipitation in the month) resulted in high amounts of incoming solar radiation (800–900 W m^{-2}) and mean maximum daily air temperature of 31.3°C. Conversely, high cloud cover in July 1993 (17 days with precipitation) resulted in lower incoming solar radiation (500–800 W m^{-2}) and

the mean maximum air temperature for the month was below 27.9°C, an unusually low value for July. In July 1995, the total monthly precipitation was 59 mm. This is still a rather low value; however, earlier in the growing season, in May and June 1995, the station received abundant rainfall and soil moisture reserves were close to field capacity by July. The incoming solar radiation was 700–850 W m^{-2} and mean maximum air temperature was 31.6°C.

For each set of experiments, LAI was changed incrementally from 0 (bare soil) to 6 (maximum LAI for crops in BATS). In all four experiments, the magnitudes of sensible and latent heat fluxes changed responding to the changes in LAI. As LAI goes up, an increase in LE is observed, as there is more leaf area to transpire (Fig. 7; only results for June 1988 are shown here). This increase is particularly noticeable at lower values of LAI (less than 3), which is consistent with observations (Kristensen 1974). An increase in latent heat flux is followed by a decrease in leaf temperature and a relative decrease in sensible heat flux. In all four experiments, leaf temperature is lower for LAI = 4 (a typical maize peak-season LAI) compared to LAI = 1 (a typical value for maize at the end of June; Fig. 8).

At lower LAI values, the partitioning of available energy appears to be, not surprisingly, a function of available water. For the same value of LAI (i.e., LAI = 1), sensible heat is generally higher than latent heat in June 1988 and lower than latent heat in July 1993. This is due to the fact that at low LAI, the role of plants in extracting soil moisture from deeper layers and releasing it through transpiration is limited and evaporation becomes an important variable determining the magnitude of latent heat flux. In June 1988, there was little soil moisture available (low precipitation in June, which was preceded by relatively dry spring). In July 1993, on the other hand, even at LAI = 1 latent heat dominates over sensible heat as there is enough water in the upper soil for evaporation to be consistently high. It can also be seen from Fig. 7 that the partitioning of energy between the sensible and latent heat fluxes was related to rainfall occurrence. On rainy days and shortly thereafter, latent heat dominated the surface energy balance, whereas during dry periods, sensible heat was the dominant component.

As leaf area index went up, stomatal resistance generally increased; it was consistently higher for LAI = 4 than for LAI = 1 (not shown here). Such stomatal behavior has to do with the fact that in BATS stomatal resistance is a function of soil moisture. At LAI = 4, plants were transpiring more water (as there was more leaf area and thus more stomates), thus depleting soil moisture faster compared to the LAI = 1 case. Under lower soil moisture (LAI = 4 case) plants were experiencing higher water stress, which resulted in partial closure of stomates (stomatal resistance went up).

Having seen a strong response of BATS to LAI changes in each of the years under consideration, we then examined the differences in BATS-simulated sensible and latent heat fluxes resulting from the inclusion of CERES growth and development functions into BATS. The same three years were considered (1988, 1993, and 1995). Each experiment was driven with observed weather data and run twice in a consecutive mode to allow for soil moisture to equilibrate, much in the same way as the experiments described above. In the first case, LAI was simulated by the standard version of BATS, BATS 1e, and in the second case, CERES-simulated LAI (more precisely, the version of BATS, BATS-GF, where CERES algorithms were used to simulate LAI, among other variables) was used. Statistical tests were performed to determine the significance levels of differences between the two simulations. These are paired *t* tests adjusted for temporal autocorrelation in the data; see Katz (1982) for details on the tests. The statistical tests were performed on daily LAI values (thus the sample size was 30 for June and 31 for July) and on 1-h latent and sensible heat fluxes and momentum flux values (thus the sample size was 720 for June and 744 for July).

Figure 9 shows leaf area index values for both experiments. The biggest difference in LAI between BATS-and CERES-simulated LAI was in 1988. It results from the fact that in BATS, LAI is a function of subsoil temperature only and does not change in response to moisture stress. In CERES, on the other hand, LAI is a function of multiple factors, including incoming solar radiation, soil temperature, soil moisture content, and soil nitrogen content (assumed to be unlimiting in these simulations). It is therefore not surprising that the biggest differences between the models come about during the drier 1988 year compared to 1993 and 1995, the years with more abundant precipitation. The differences in LAI between the two simulations are statistically significant with over 99% confidence levels (p − values <0.01) for all four months.

Figure 10 shows the sensible and latent heat fluxes simulated by BATS with (a) LAI simulated with the standard version of BATS, BATS le; and (b) LAI simulated by CERES development and growth functions within the modified version of BATS, BATS-GF. Again, the biggest differences between the two cases are seen in June and July of 1988. The mean difference in latent heat flux between the two cases (BATS - BATSGF) was 21.5 W m^{-2} in June 1988 and 19.0 W m^{-2} in July 1988, both rather high values. The mean differences in sensible heat flux were −15.1 W m^{-2} in June 1988 and −13.7 W m^{-2} in July 1988. The smallest difference is seen in July 1993, −3.4 W m^{-2} for sensible heat flux and 4.6 W m^{-2} for latent heat flux. In July 1995, the mean difference in sensible heat flux between the two simulations was −5.1 W m^{-2} and the mean difference in latent heat flux was 6.8 W m^{-2}. The differences in sensible and latent heat fluxes between the two simulations were statistically significant with over 99% confidence levels (p−values <0.01) for all four months.

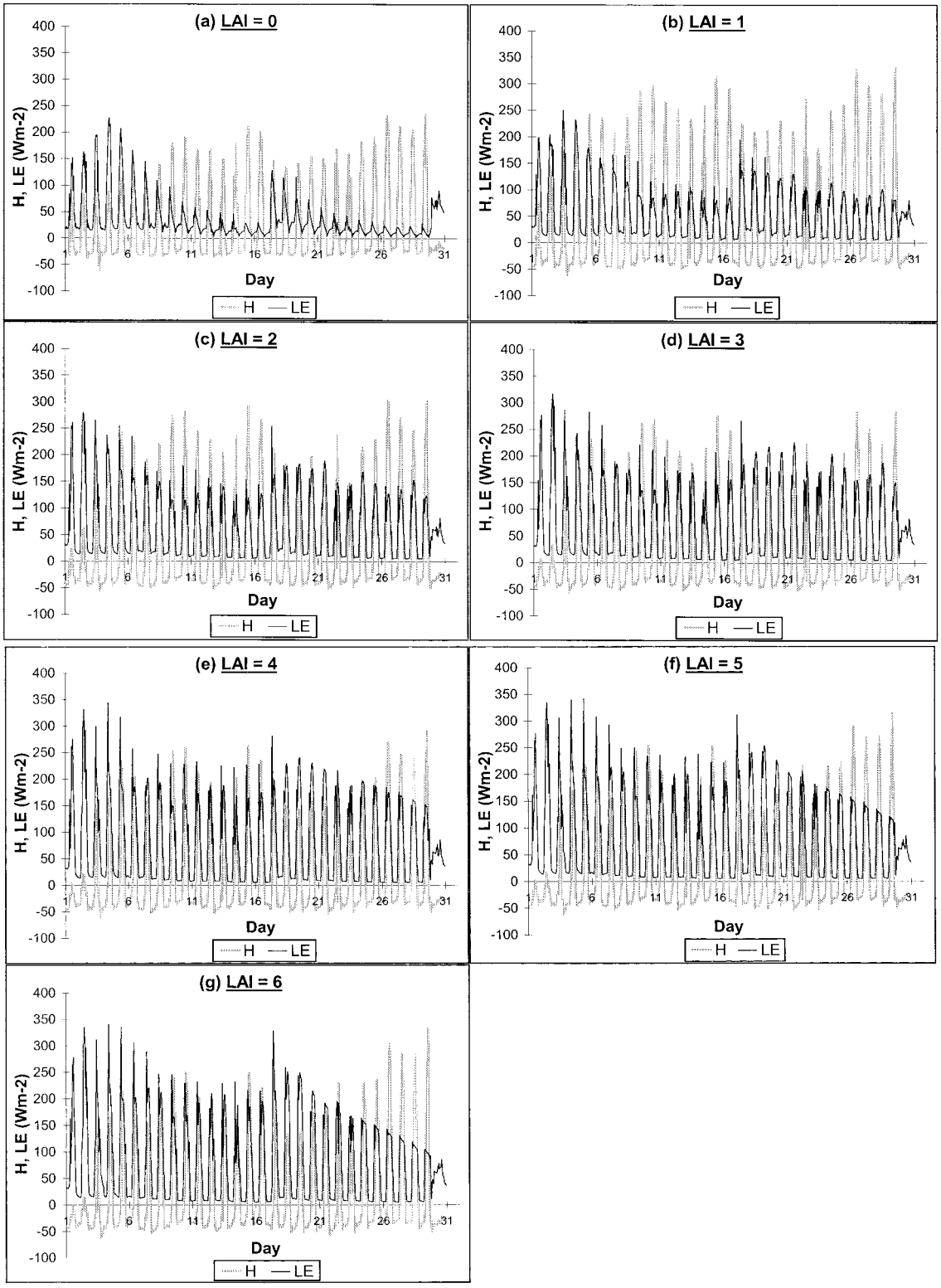

FIG. 7. BATS-simulated sensible (H) and latent (LE) heat fluxes for Jun 1988.

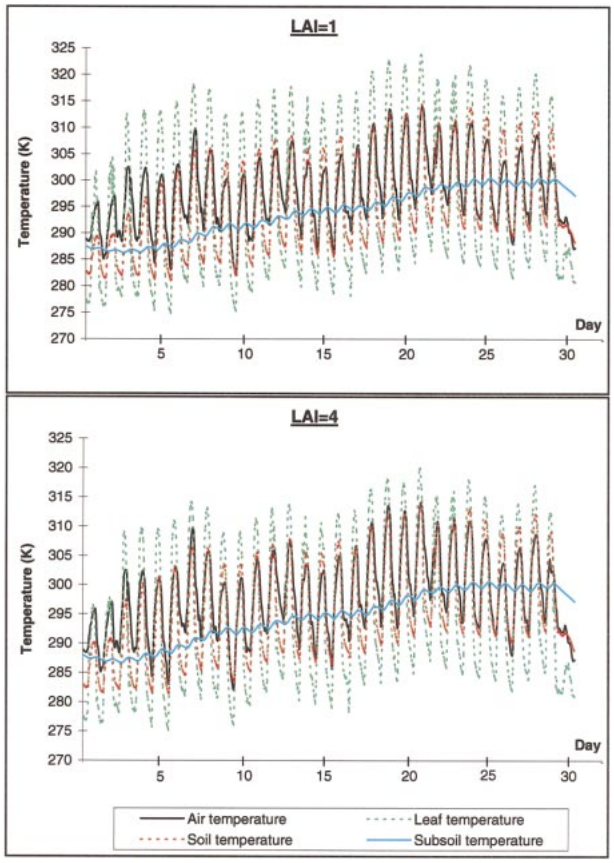

FIG. 8. BATS-simulated air, leaf, soil, and subsoil temperatures for Jun 1988 in Grand Island, NE.

Differences were largest during the afternoon hours and smallest at night.

Besides the effect on the magnitude of latent heat flux, LAI has an effect on the relative contributions of transpiration and evaporation to the net latent heat flux (Fig. 11). It can be seen that in July 1988, transpiration was unrealistically high in the BATS-generated LAI scenario and dominated over evaporation. For the same period of time when CERES-generated LAI was used, not only did the magnitude of latent heat flux decrease significantly, but also evaporation became the dominant factor determining latent heat flux. In July 1993, a different situation is seen. In both BATS- and CERES-generated LAI cases, transpiration dominated over evaporation in terms of the relative contributions to latent heat flux. The magnitude of transpiration was somewhat higher in case of BATS-generated LAI, by a mean monthly value of 5.3 W m^{-2}. In July 1995, transpiration also seemed to dominate over evaporation, but the difference between the two cases was higher than in July 1993, a mean monthly difference of 11.1 W m^{-2}.

c. Sensitivity of BATS-simulated momentum flux to canopy height

We introduced a series of equations into both CERES and BATS models to calculate maize canopy height. The equations were taken from the ALMANAC model (Kiniry et al. 1997; Spanel and Taylor 1996) and are given below:

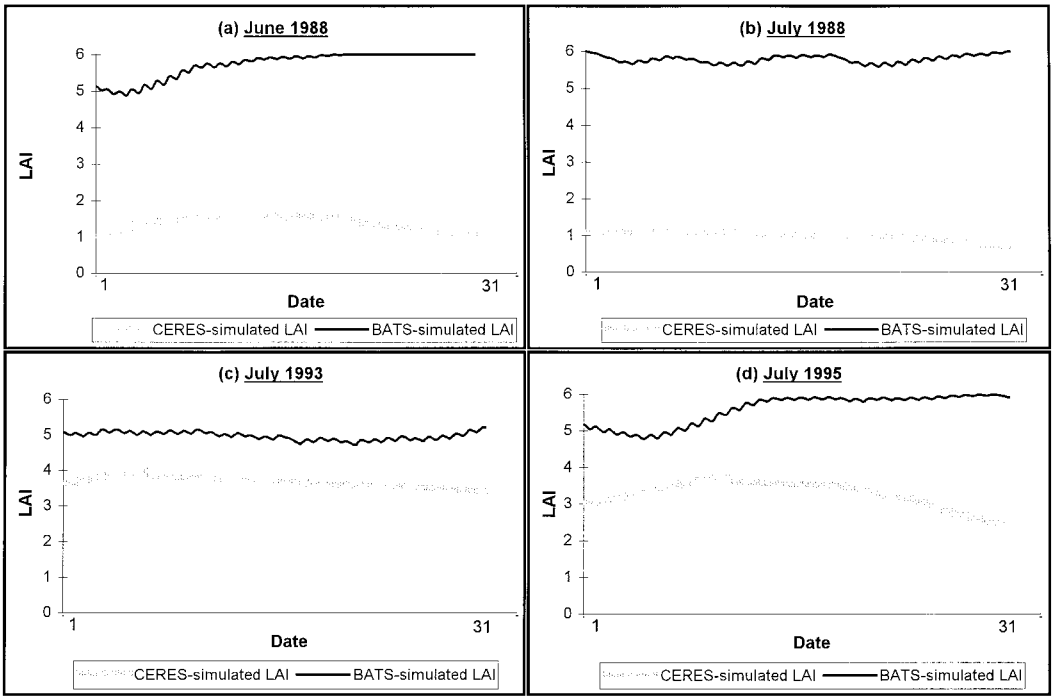

FIG. 9. CERES-simulated LAI and BATS-simulated LAI.

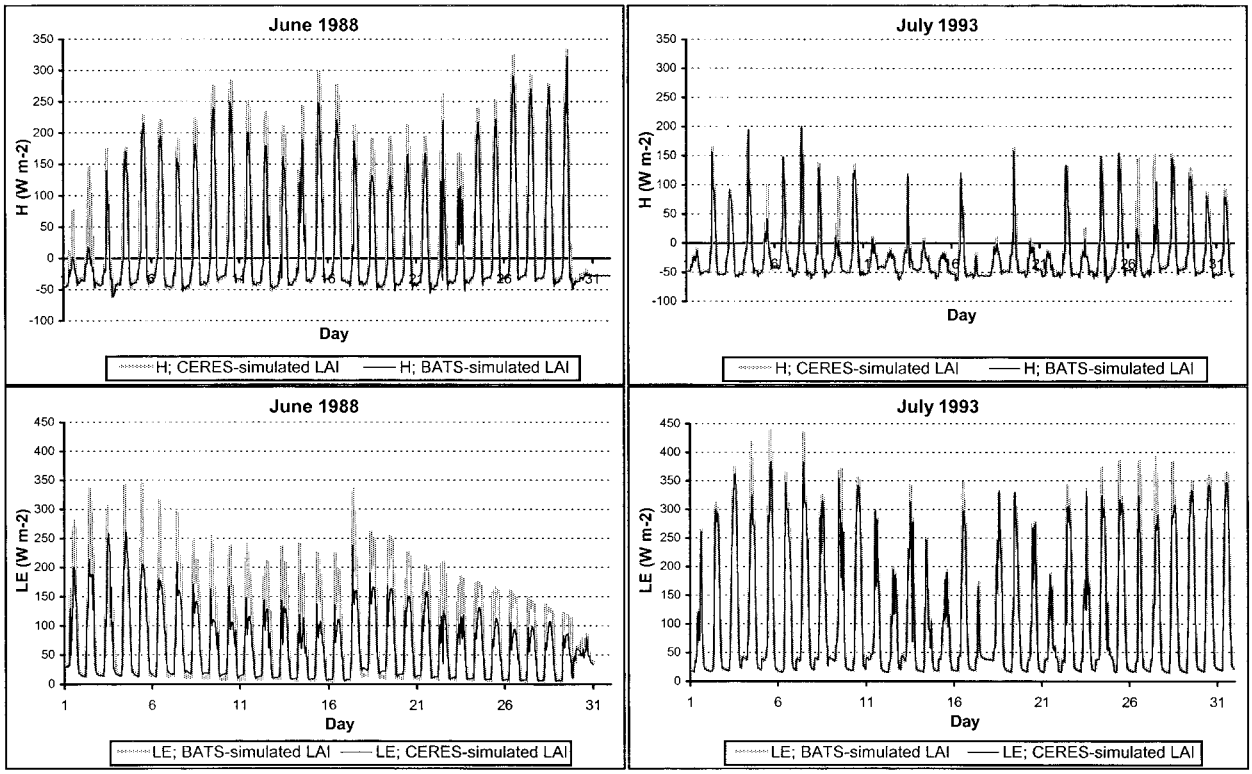

FIG. 10. BATS-simulated sensible and latent heat fluxes for Jun 1988 and Jul 1993.

$$F = \frac{\text{syp}}{\text{syp} + \exp(3.0551 - 13.3855\text{syp})},$$

$$\text{cht} = \text{hmx}\sqrt{F + 1 \times 10^{-10}}.$$

Here syp is the fraction of the heat units to maturity that has accumulated by a given day of simulation; hmx is the maximum height (we used hmx = 2.0 m); and cht is height on a given day of simulation.

To account for the effect of moisture stress on canopy height increase, we assumed that if the soil water deficit factor, SWFAC, was equal to or less than 0.5, no daily accumulation of plant height was achieved. Such an assumption is based on Penning de Vries et al. (1989). CERES-simulated maximum plant height generally varied between 1.8 m and 2 m, and during the drought years (1988, 1989) was significantly less (Fig. 12).

In the following set of experiments, we examined the sensitivity of BATS-simulated momentum flux to changes in roughness length associated with the seasonal changes in maize canopy height. In BATS, the momentum flux is a function of wind speed above the canopy, surface roughness length, and atmospheric stability (which is a function of the Richardson number, R_i). The R_i is defined as

$$R_i = \frac{g(\partial\theta/\partial z)}{T(\partial v/\partial z)^2}.$$

Here, g is the acceleration due to gravity; $\partial\theta/\partial z$ and $\partial v/\partial z$ are the vertical gradients of mean potential temperature and mean horizontal wind speed; and T is the mean absolute temperature (K).

Figure 13 gives hourly values of above-canopy wind speed observed by the AWDN station in Grand Island that were used to drive the model. The wind speed values range between about 0 and 10 m s^{-1} with gusts on one day in July 1993 of up to 16 m s^{-1}. The wind speeds are generally lower at night than during daytime. July 1993 is characterized with the lowest and June 1988 the highest wind speeds for the four sets of experiments. We ran BATS twice for each of the years 1988, 1993, and 1995 (same as in section 5.2) and used two values of roughness length (z_0 = 0.06 m and z_0 = 0.2 m) to initialize the model. The ratios of surface roughness length to canopy height generally found in the literature are 0.14 to 0.10 (Dorman and Sellers 1989; Monteith and Unsworth 1990). Therefore, surface roughness length of 0.06 m (the standard BATS value for agroecosystems) would correspond to canopy height of about 0.6 m and surface roughness length of 0.2 m would correspond to canopy height of about 2 m (a typical peak growth height for maize). Figure 14 shows momentum fluxes simulated for each case.

The momentum flux values range between about 0 (on calm days and at night) to about 0.1–0.6 N m^{-2} for z_0 = 0.06 m and up to about 0.4–0.8 N m^{-2} for z_0 = 0.2 m. The diurnal cycle in momentum flux is due to

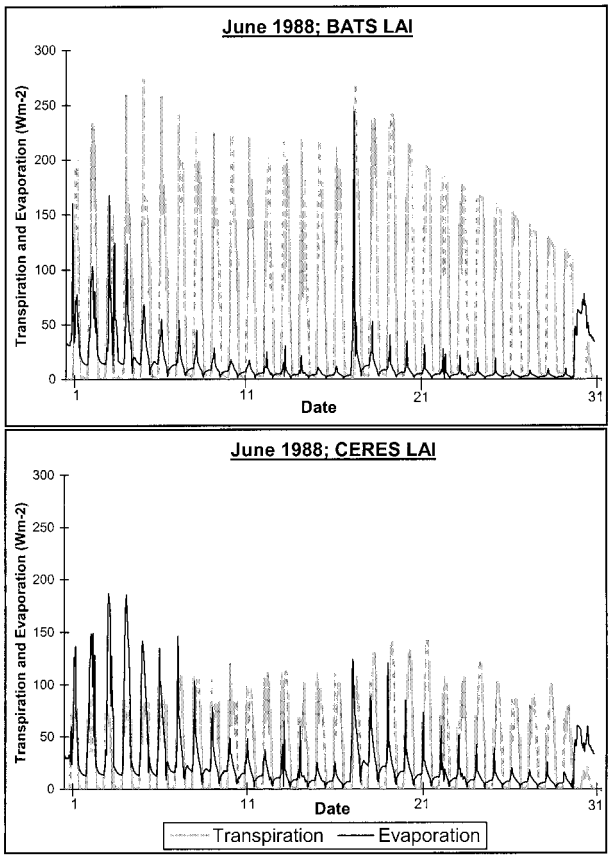

FIG. 11. Transpiration and evaporation in Jun 1988.

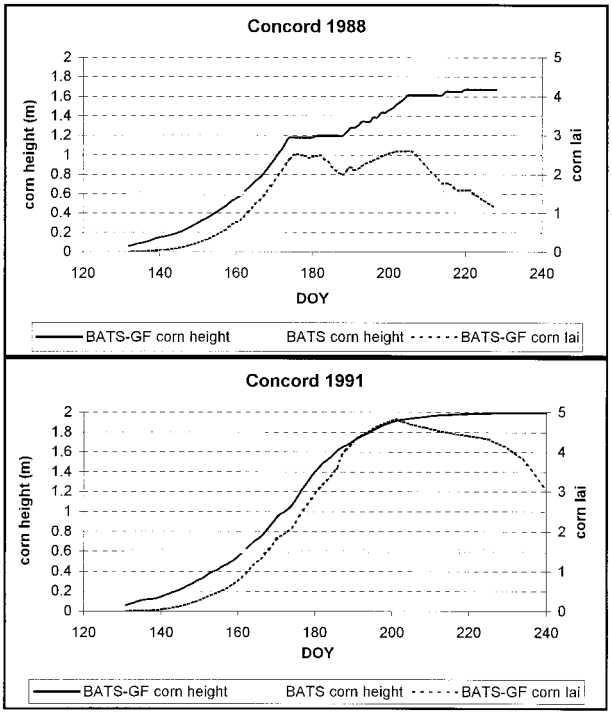

FIG. 12. CERES-simulated corn height and LAI for Concord, NE.

the diurnal cycle of the difference between the surface and the air temperatures, which define the bulk Richardson number. There are significant differences (up to 100%) in momentum flux between the two roughness

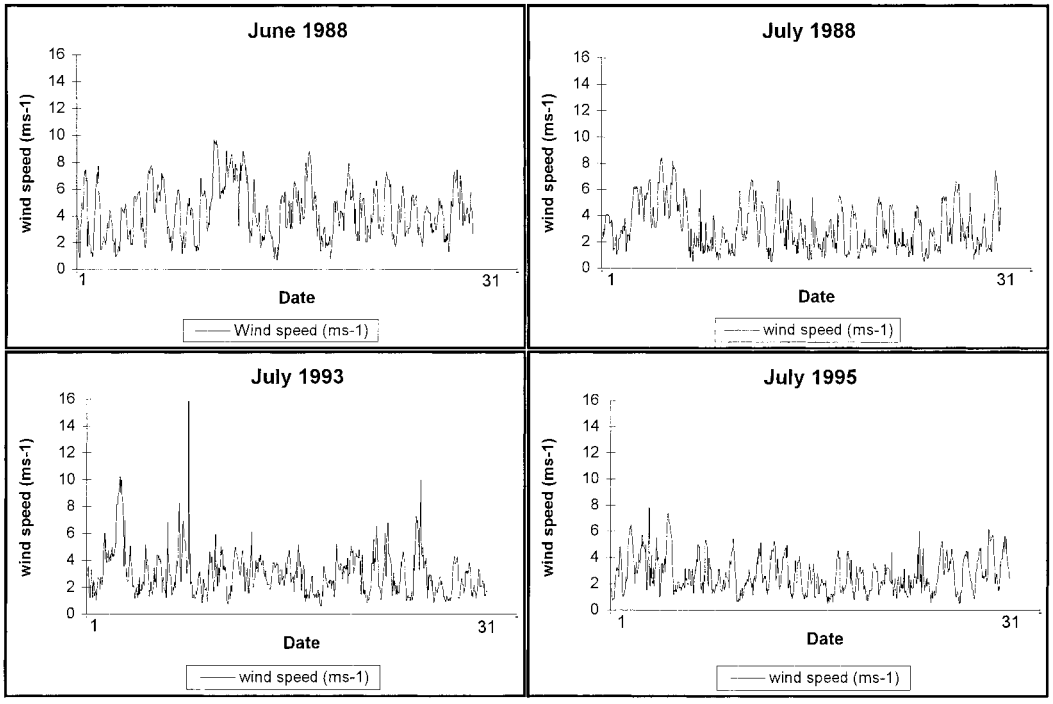

FIG. 13. Observed wind speed (at $z = 1.5$ m) for Grand Island, NE.

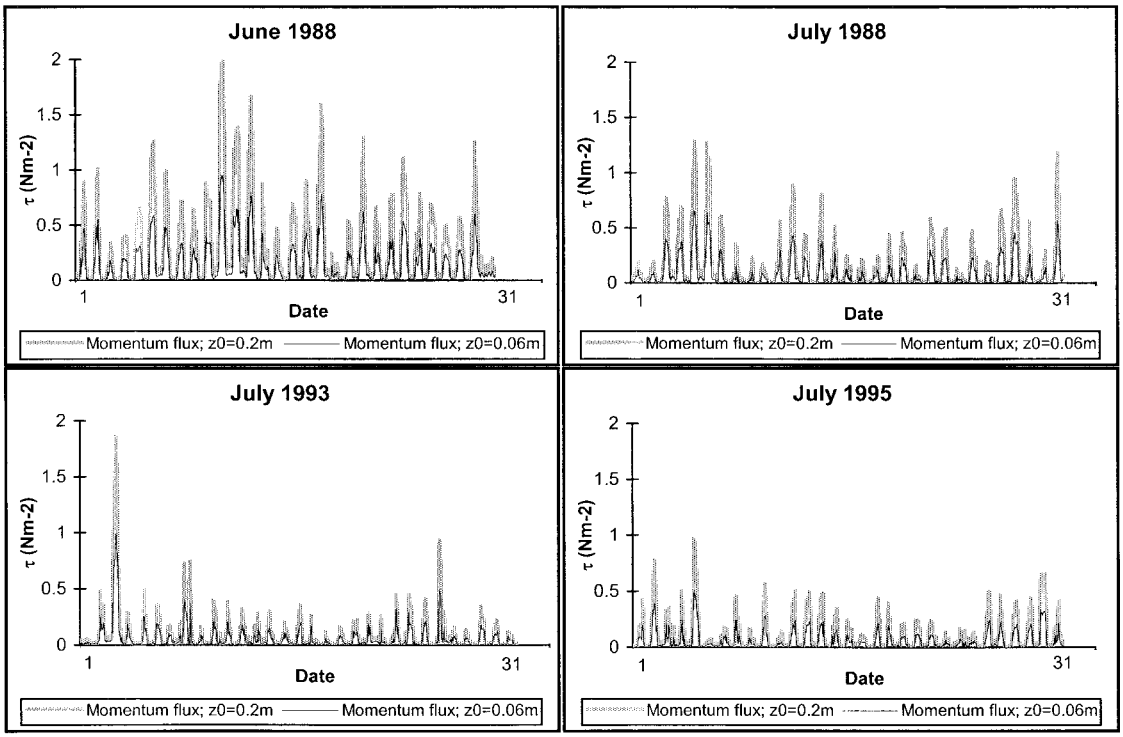

FIG. 14. BATS-simulated momentum flux (τ) for Grand Island, NE.

length scenarios. In all four cases, momentum flux is higher when $z_0 = 0.2$ m compared to the case of $z_0 = 0.06$ m. The highest momentum flux values in both cases were simulated for June 1988, when the combination of wind speed, and surface and air temperatures created the most unstable conditions. July 1993 and July 1995 had the lowest values of momentum flux associated generally with lower wind speeds and highest atmospheric stability. The ratio of friction velocity to mean wind speed (for wind speeds in excess of 2 m s^{-1}) varied from 0.055 in July 1993 to 0.064 in July 1995 for $z_0 = 0.06$ m. For $z_0 = 0.2$ m case, this ratio was generally higher, between 0.080 and 0.093.

6. Summary and conclusions

In this paper, we introduced a crop growth model (CERES v3.0) and a biophysical model (BATS), which, when interactively coupled, can quantify the effect of seasonal and interannual variability in crops on the sensible and latent heat fluxes and on the partitioning of the available energy between them. We found substantial differences in surface fluxes of sensible heat, latent heat, and momentum between the current version of BATS (BATS 1e) and the interactive version, BATS-GF. Changes of up to 35% in *H* and 45% in LE were simulated when LAI was changed from 1 to 4. Relative contributions of evaporation and transpiration to the latent heat flux were also significantly affected by these LAI changes. We also note that in this study, BATS-simulated *H* and LE responded most dramatically to incremental LAI changes at values below 4. These findings are generally consistent with results of other researchers (Bonan et al. 1993; Pitman 1994; Gao et al. 1996; Xue et al. 1996). Up to 100% changes in momentum flux were simulated in response to canopy height change from 0.6 m (value used in BATS 1e for crops) to 2.0 m (typical value for corn at maturity).

The results of our experiments presented in this paper point to the importance of interactively modeling vegetation growth for determining surface fluxes of heat, moisture, and momentum. This may be most important in years of moisture stress (such as 1988 and 1989 in the Great Plains) and also appears to influence the interannual variability of simulated fluxes (interannual variability in *H* and LE was higher in the interactive compared to control simulations). Further experiments were conducted to investigate the effect of simulated changes in surface fluxes on mesoscale atmospheric circulations. The results of such coupled experiments are presented in the follow-up paper, Part II.

Acknowledgments. We wish to thank Dr. John Lindquist of the University of Nebraska for providing field data on maize development and growth for model validation. We also thank Larry McDaniel of the National Center for Atmospheric Research for technical and computer support. We acknowledge the High Plains Climate Center of the University of Nebraska for providing the data set of observed climate for the Great Plains used

in this study. We acknowledge the National Drought Mitigation Center of the University of Nebraska for providing the data for the Standardized Precipitation Index. Finally, we thank Dr. A. Weiss of the University of Nebraska and anonymous reviewers for useful editorial comments. The National Center for Atmospheric Research is sponsored by the National Science Foundation.

REFERENCES

Beljaars, A. C. M., P. Viterbo, M. J. Miller, and A. K. Betts, 1996: The anomalous rainfall over the United States during July 1993: Sensitivity to land surface parameterization and soil moisture anomalies. *Mon. Wea. Rev.*, **124,** 362–383.

Betts, A. K., J. H. Ball, and A. C. M. Beljaars, 1993: Comparison between the land surface response of the ECMWF model and the FIFE-1987 Data. *Quart. J. Roy. Meteor. Soc.*, **119,** 975–1001.

Bonan, G. B., 1996: A land surface model (LSM Version 1.0) for ecological, hydrological, and atmospheric studies: Technical description and user's guide. NCAR Tech. Note 417, 150 pp.

——, 1997: Effects of land use on the climate of the United States. *Climatic Change,* **37,** 449–486.

——, D. Pollard, and S. L. Thompson, 1993: Influence of subgrid-scale heterogeneity in leaf area index, stomatal resistance, and soil moisture on grid-scale land–atmosphere interactions. *J. Climate,* **6,** 1882–1897.

Chase, T. N., R. A. Pielke Sr., T. G. F. Kittel, J. S. Baron, and T. J. Stohlgren, 1999: Potential impacts on Colorado Rocky Mountain weather due to land use changes on the adjacent great plains. *J. Geophys. Res.,* **104,** 16 673–16 690.

Ciais, P., P. P. Tans, M. Trolier, J. W. C. White, and R. J. Francey, 1995: A large northern hemisphere terrestrial CO_2 sink indicated by the $^{13}C/^{12}C$ ratio of atmospheric CO_2. *Science,* **269,** 1098–1102.

Clapp, R. B., and G. M. Hornberger, 1978: Empirical equations for some soil hydraulic properties. *Water Resour. Res.,* **14,** 601–604.

Collatz, G. J., L. Bounoua, and P. J. Sellers, 1993: SiB: Documentation and Fortran code listing. Version 1. GSFC/NASA Tech. Note, 12 pp.

Copeland, J. H., T. N. Chase, J. Baron, T. G. F. Kittel, and R. A. Pielke, 1996: Impacts of vegetation change on regional climate and downscaling of GCM output to the regional scale. *Regional Impacts of Global Climate Change: Assessing Change and Response at the Scales that Matter,* S. J. Ghan, et al., Eds., Battelle Press, 199–212.

Cuenca, R. H., M. Ek, and L. Mahrt, 1996: Impact of soil water property parameterization on atmospheric boundary layer simulation. *J. Geophys. Res.,* **101,** 7269–7277.

Dickinson, R. E., A. Henderson-Sellers, and P. J. Kennedy, 1993: Biosphere–atmosphere transfer scheme (BATS) Version 1e as Coupled to the NCAR Community Climate Model. NCAR Tech. Note 387, 72 pp.

——, M. Shaikh, R. Bryant, and L. Graumlich, 1998: Interactive canopies for a climate model. *J. Climate,* **11,** 2823–2836.

Dirmeyer, P. A., 1994: Vegetation stress as a feedback mechanism in midlatitude drought. *J. Climate,* **7,** 1463–1483.

Dorman, J. L., and P. J. Sellers, 1989: A global climatology of albedo, roughness length, and stomatal resistance for atmospheric general circulation models as represented by the simple biosphere model (SiB). *J. Appl. Meteor.,* **28,** 833–855.

Ek, M., and R. H. Cuenca, 1994: Variation in soil parameters: implications for modeling surface fluxes and atmospheric boundary-layer development. *Bound.-Layer Meteor.,* **70,** 369–383.

Foley, J. A., I. C. Prentice, N. Ramankutty, S. Levis, D. Pollard, S. Sitch, and A. Haxeltine, 1996: An integrated biosphere model of land surface processes, terrestrial carbon balance, and vegetation dynamics. *Global Biogeochem. Cycles,* **10,** 603–628.

Gao, X., S. Sorooshian, and H. V. Gupta, 1996: Sensitivity analysis of the biosphere–atmosphere transfer scheme. *J. Geophys. Res.,* **101** (D3), 7279–7289.

Hubbard, K. G., 1994: Spatial variability of daily weather variables in the high plains of the USA. *Agric. For. Meteor.,* **68,** 29–41.

Jones, C. A. and J. R. Kiniry, Eds., 1986: *CERES-Maize: A Simulation Model of Maize Growth and Development.* Texas A&M University Press, 194 pp.

Katz, R. W., 1982: Statistical evaluation of climate experiments with general circulation models: A parametric time series modeling approach. *J. Atmos. Sci.,* **39,** 1446–1455.

Kim, J., and S. Verma, 1990: Components of surface energy balance in a temperate grassland ecosystem. *Bound.-Layer Meteor.,* **51,** 401–417.

Kiniry, J. R., and Coauthors, 1997: Evaluation of two maize models for nine U.S. locations. *Agron. Journal,* **89,** 421–426.

Kristensen, K. J., 1974: Actual evapotranspiration in relation to leaf area. *Nordic Hydrol.,* **5,** 173–182.

Lindquist, J. L., 1997: An ecophysiological approach to understanding corn tolerance and velvetleaf suppressive ability. Ph.D. dissertation, University of Nebraska, 156 pp.

Lu, L., R. A. Pielke Sr., G. E. Liston, W. J. Parton, D. Ojima, and M. Hartman, 2001: Implementation of a two-way interactive atmospheric and ecological model and its application to the central United States. *J. Climate,* **14,** 900–919.

McKee, T. B., N. J. Doesken, and J. Kleist, 1993: The relationship of drought frequency and duration to timescales. Preprints, *Eighth Conf. on Applied Climatology,* Anaheim, CA, Amer. Meteor. Soc., 179–184.

Mearns, L. O., C. Rosenzweig, and R. Goldberg, 1996: The effect of changes in daily and interannual climatic variability on CERES-Wheat: A sensitivity study. *Climatic Change,* **32,** 257–292.

——, ——, and ——, 1997: Mean and variance change in climate scenarios: Methods, agricultural applications, and measures of uncertainty. *Climatic Change,* **35,** 367–396.

——, T. Mavromatis, E. Tsvetsinskaya, C. Hays, and W. E. Easterling, 1999: Comparative responses of EPIC and CERES crop models to high and low spatial resolution climate change scenarios. *J. Geophys. Res.,* **104,** 6623–6646.

Monteith, J. L., and M. N. Unsworth, 1990: *Principles of Environmental Physics.* 2d ed. Edward Arnold, 291 pp.

Olson, J. S., J. A. Watts, and L. J. Allison, 1983: *Carbon in Live Vegetation of Major World Ecosystems.* U.S. Department of Energy, 152 pp.

Pang, X. P., J. Letey, and L. Wu, 1997: Yield and nitrogen uptake prediction by CERES-Maize model under semiarid conditions. *Soil Sci. Soc. Amer. J.,* **61,** 254–256.

Penning de Vries, F. W. T., D. M. Jansen, H. F. M. ten Berge, and A. Bakema, 1989: *Simulation of Ecophysiological Processes of Growth in Several Annual Crops.* PUDOC.

Pitman, A. J., 1994: Assessing the sensitivity of a land-surface scheme to the parameter values using a single column model. *J. Climate,* **7,** 1856–1869.

Pollard, D. and S. L. Thompson, 1995: Use of a land-surface-transfer scheme (LSX) in a global climate model: The response to doubling stomatal resistance. *Global Planet. Change,* **10,** 129–161.

Priestley, C. H. B., and R. J. Taylor, 1972: On the assessment of surface head flux and evaporation using large-scale parameters. *Mon. Wea. Rev.,* **100,** 81–92.

Rosenzweig, C., 1990: Crop response to climate change in the Southern Great Plains: A simulation study. *Prof. Geographer,* **42,** 20–37.

Schwartz, M. D., 1992: Phenology and springtime surface-layer change. *Mon. Wea. Rev.,* **120,** 2570–2578.

——, and T. R. Karl, 1990: Spring phenology: Nature's experiment to detect the effect of ''green-up'' on surface maximum temperature. *Mon. Wea. Rev.,* **118,** 883–890.

Sellers, P. J., 1992: Biophysical models of land surface processes.

Climate System Modeling, K. E. Trenberth Ed., Cambridge University Press, 451–490.

——, Y. Mintz, Y. C. Sud, and A. Dulcher, 1986: A simple biosphere model (SiB) for use within general circulation models. *J. Atmos. Sci.,* **43,** 505–531.

——, J. A. Berry, G. J. Collatz, C. B. Field, and F. G. Hall, 1992: Canopy reflectance, photosynthesis, and transpiration. III. A reanalysis using enzyme kinetics–electron transport models of leaf physiology. *Remote Sens. Environ.,* **42,** 187–216.

Spanel, D., and D. Taylor, 1996: Quick start on almanac. USDA-Agricultural Research Service and Texas Agricultural Experiment Station, 30 pp.

Trenberth, K. E. and G. W. Branstator, 1992: Issues in establishing causes of the 1988 drought over the North America. *J. Climate,* **5,** 159–172.

——, and C. J. Guillemot, 1996: Physical processes involved in the 1988 drought and 1993 floods in North America. *J. Climate,* **9,** 1288–1298.

Tsuji, G. Y., G. Uehara, and S. Balas, Eds., 1994: DSSAT Version 3. University of Hawaii.

Tsvetsinskaya, E., L. O. Mearns, and W. E. Easterling, 1999: Investigating the effect of seasonal plant growth and development in 3-dimensional atmospheric simulations. *Proc. Ninth Int. Offshore and Polar Engineering Conf.,* Brest, France, International Society of Offshore and Polar Engineers, 382–389.

Verma, S. B., J. Kim, and R. J. Clement, 1992: Momentum, water vapor, and carbon dioxide exchange at a centrally located prairie site during FIFE. *J. Geophys. Res.,* **97,** 18 629–18 639.

Verseghy, D. L., N. A. McFarlane, and M. Lazare, 1993: CLASS—A Canadian land surface scheme for GCMs: Vegetation model and coupled runs. *Int. J. Climatol.,* **13,** 347–370.

Viterbo, P., and A. C. M. Beljaars, 1995: An improved land surface parameterization scheme in the ECMWF model and its validation. *J. Climate,* **8,** 2716–2748.

Webb, R. S., C. E. Rosenzweig, and E. R. Levine, 1991: A global dataset of soil particle size properties. NASA Tech. Memo. 4286, 32 pp.

Williams, J. R., P. T. Dyke, and C. A. Jones, 1982: EPIC—A model for assessing the effects of erosion on soil productivity. *Proc. Int. Conf. on State of the Art in Ecological Modeling,* Colorado State University, Fort Collins, CO.

Xue, Y., M. J. Fennessy, P. J. Sellers, 1996: Impact of vegetation properties on U.S. summer weather prediction. *J. Geophys. Res.,* **101,** 7419–7430.

Zobler, L., 1986: A world soil file for global climate modeling. NASA Tech. Memo. 87802, 32 pp.